

submitted to *The Astrophysical Journal***A Possible Detection of M31* with *Chandra***Michael R. Garcia¹, Benjamin F. Williams¹, Feng Yuan², Albert K. H. Kong¹, F. A. Primini¹, P. Barmby¹, P. Kaaret³, and Stephen S. Murray¹**ABSTRACT**

Two independent sets of *Chandra* and HST images of the nuclear region of M31 allow registration of X-ray and optical images to $\sim 0.1''$. This registration shows that none of the bright ($\sim 10^{37}\text{erg s}^{-1}$) X-ray sources near the nucleus is coincident with the central super-massive black hole, M31*. A 50ks *Chandra* HRC image shows 2.5σ evidence for a faint ($3 \times 10^{35}\text{erg s}^{-1}$), apparently resolved source which is consistent with the position of the M31*. The Bondi radius of M31* is $0.9''$, making it one of the few super-massive black holes with a resolvable accretion flow. This large radius and the previous detections of diffuse, X-ray emitting gas in the nuclear region make M31* one of the most secure cases for a radiatively inefficient accretion flow and place some of the most severe constraints on the radiative processes in such a flow.

Subject headings: accretion — black hole physics — galaxies: individual (M31)
— galaxies: nuclei

1. Introduction

It is now accepted that a supermassive black hole (SMBH) is present in essentially every galactic core (Magorrian et al. 1998). However, most galactic nuclei appear inactive, raising

¹Harvard-Smithsonian Center for Astrophysics, 60 Garden Street, Cambridge, MA 02138; williams@head-cfa.harvard.edu; garcia@head-cfa.harvard.edu; akong@head-cfa.harvard.edu; fap@head-cfa.harvard.edu; ssm@head-cfa.harvard.edu

²Department of Physics, Purdue University, 525 Northwestern Avenue, West Lafayette, IN 47907; fyuan@physics.purdue.edu

³Department of Physics and Astronomy, University of Iowa, Iowa City, IA 52242-1479, philip-kaaret@uiowa.edu

the question: “Why are these SMBHs such embarrassingly faint X-ray sources, as compared to the SMBHs previously known to exist in AGN?” Explanations fall into two broad classes - either the accretion rate is extremely low, i.e., the SMBHs are ‘starved’, or the accretion process is radiatively inefficient. A straightforward way to determine which explanation is correct is to resolve the accretion flow and therefore securely determine the mass accretion rate. We note that hybrid explanations are possible, ie, the flow could start at the Bondi rate and then be slowed or stopped by winds, convection, and/or magnetic fields (Perna et al. 2003).

Because of the limited resolution of current X-ray telescopes the only currently known examples of resolved accretion flows into SMBHs are those in Sgr A* (Baganoff et al. 2003) and M87 (Di Matteo et al. 2003). Assuming the accretion flow in Sgr A* has the “normal” accretion efficiency, its expected luminosity would be roughly seven orders of magnitude greater than the observed value. So we cannot escape the conclusion that the accretion flow in Sgr A* is radiatively inefficient (Yuan et al. 2003). M87 is under-luminous only by four (not seven) orders of magnitude so must also have a radiatively inefficient flow but the presence of a strong and resolved nuclear jet complicates the picture.

At a distance of 780 kpc (Stanek & Garnavich 1998; Macri et al. 2001), M31* is the nearest analog to Sgr A*. In addition to its highly unusual double nucleus, the center of M31 houses a $3 \times 10^7 M_{\odot}$ black hole (Kormendy & Bender 1999) spatially coincident with the point radio source M31* (Crane et al. 1992). The radio source is unresolved at the $\sim 0.35'' \sim 1\text{pc}$ level. While M31* is 100x further away than Sgr A*, it suffers much less reddening: $A_V \sim 1$ (Garcia et al. 2000), whereas $A_V \sim 30$ for Sgr A*.

The first *Chandra* observations of M31 led us to associate a super-soft source near M31* with this SMBH (Garcia et al. 2000). Subsequently we were able to register several HST WFPC2 images of the nuclear region with our ACIS mosaic using two globular clusters, reducing the error circles of the X-ray sources by a factor of ~ 10 . This showed that our initial association was incorrect, and that none of the bright ($L_X \sim 10^{37}\text{erg s}^{-1}$) sources near the center of the galaxy is spatially coincident with M31* (Garcia et al. 2001). Recently we have obtained an HST ACS image which fortuitously contains M31*. Registration of this image with a *Chandra* HRC image confirms our earlier results, and suggests that a previously unresolved faint source may be co-incident with M31*. In this paper we present both datasets and discuss M31* in the context of other low-luminosity SMBH.

2. Observations

The absolute astro-metric accuracy of both *Chandra* and HST images is only $\sim 1''$, but by using common sources one can register the images to $\sim 0.1''$. As globular clusters are some of the most common X-ray point sources found in M31 and are easily identifiable on HST images, we searched for clusters near the nucleus which could provide the desired registration. We found two such clusters.

Below we show that we were then able to accurately register two completely independent datasets, one using the HST/WFPC2 and the *Chandra*/ACIS-I, and the other using the HST/ACS and the *Chandra*/HRC. Both confirm that none of the bright ($L_X \sim 10^{37} \text{erg s}^{-1}$) sources near the nucleus are coincident with M31*. The HRC image shows marginal evidence for a weak, resolved X-ray source at the position of M31*. While the ACIS observations do not show a resolved source, they are consistent with a source of the same flux at the M31* position.

2.1. HST WF/PC2 and Chandra ACIS Observations

The *Chandra* observations of the nuclear region analyzed herein consist of 7 separate ACIS observations taken during the first two years of *Chandra* operations, which have been summed to generate an image with an effective exposure time of 34.7 ks. These observations are described in detail by Kong et al. (2002), who considered these 7 and one additional (OBSID 1583) observation. In order to maintain the highest possible spatial resolution in the summed image, the individual images were first generated in $1/8''$ pixels, with the standard $\pm 1/4''$ position randomization removed. The images were then stacked using the positions of the point X-ray sources as registration marks. The resulting image has a radially averaged FWHM on axis of $\sim 0.6''$ as determined by IRAF¹ (imexam) profile fitting on numerous sources. We limited the image size to 2048^2 pixels, therefore covering $4.2' \times 4.2'$. The central region of this image is shown in Figure 1. Two of the three bright nuclear sources are visible in this image, including the northernmost source (N1 = CXOM31 J004244.3+411608/ r1-10) and the central super-soft source (SSS = CXOM31 J004244.3+411607/ r1-9, Kong et al. 2002).

An archival WFPC2 image which includes M31* also includes a recently discovered

¹IRAF is distributed by the National Optical Astronomy Observatory, which is operated by the Association of Universities for Research in Astronomy, Inc., under cooperative agreement with the National Science Foundation.

globular cluster (M31GC J004246+411737) identified by Barmby & Huchra (2001). This archival image was taken with the F300W filter (central wavelength 3000Å, bandpass 300Å) on 1995 June 19. We obtained a WFPC2 image on 2000 Feb 02 in order to search for a UV counterpart the the new *Chandra* X-ray transient CXOM31 J004242.1+411608 (Murray et al. 1999; Kong et al. 2002; also called CXO J004241.0+411608 in Garcia et al. 2000). This image was taken with the F336W filter (central wavelength 3360Å, bandpass 200Å) and also includes M31*, as well as the cluster mita213 in the catalog of Magnier (1993). Both of these globular clusters are also detected in the merged ACIS-I image, as sources r2-15 and r1-32 in Kong et al. (2002).

These two HST images were taken at orientations that differ by nearly 180°, allowing them to cover the maximal area of M31, while still allowing partial overlap of the PC and WFC chips. In these overlapping regions we identified > 100 individual point sources, which we used to register the two images to a common frame. We arbitrarily choose the frame of the F300W image as determined by the HST pipeline processing as our preferred reference frame. The registration of the two WFPC2 images was done with standard IRAF routines (mkpattern, ccsetwsc, wregister, imcombine, geomap, geotran, wscopy; as described on the wregister help page) and has a rms error of 0.05". The mosaic of F300W and F336W images covers approximately 3' × 3'. The central region of the F300W PC chip was centered on M31* and the central part of this PC image is show in Figure 2. The ACIS contours from Figure 1 are overlaid.

2.1.1. Registering the WFPC2 and ACIS Images

The errors in the registration of the *Chandra* image to the HST frame are dominated by the positional uncertainties of the globular clusters as measured in the *Chandra* image. These errors are $r = FWHM / (2.3 * \sqrt{N})$ where N is the number of counts in each cluster. From the images, we measure $r = 0.06''$ for mita213 (with 59 counts) and $r = 0.07''$ for M31GC J004246+411737(with 39 counts). We note that the *Chandra* wavedetect tool gives similar errors.

Of course, the position of the globular clusters within the HST image also has some error. The *FWHM* of the images of these clusters themselves, as measured from the HST images is 0.50" for mita213 and 0.35" for M31GC J004246+411737. However, the much larger number of counts in the HST images ($\gtrsim 10,000$) indicates these position errors are $\lesssim 0.01''$. Summing the rms of the HST fit and the errors for the two clusters used for registration in quadrature indicates a 1σ error for position determination of 0.082" which we conservatively round to 0.1". We note that this registration was done with a simple translation. We did not

find any errors in roll or scale factor, which indicates they are smaller than our computed registration error.

2.2. HST ACS and *Chandra* HRC Observations

An HST ACS image of the M31 nucleus was obtained by us on 2004 Jan 23 as part of our *Chandra* AO5 program searching for the optical counterparts of black hole X-ray novae in M31. The 2200 second image was obtained with the F435W (=B band) filter in a standard 4 point dither pattern and reduced with standard HST drizzle tools. Figure 3 shows the region of this image surrounding M31*, overlaid with X-ray contours from the archival 47 ks HRC-I observation shown in Figure 4 (OBSID 1912, obtained on 2001 Nov 1, see Kaaret 2002). The contours in Figure 3 show the super-soft source (SSS) on the bottom with source N1 above it. Approximately 0.5'' to the right a separate contour is seen overlaying M31*.

Figure 4 shows the 47ks HRC image at its intrinsic 1/8''/pixel scale. At a position consistent with M31* there appears to be a weak source which is resolved from N1 and SSS. There are 13 counts within a 3 pixel diameter circle, which when assuming the typical M31 source spectrum of $N_{\text{H}} = 7 \times 10^{21} \text{cm}^{-2}$ and $\alpha = 1.7$ corresponds to a luminosity of $L_{\text{X}} = 3 \times 10^{35} \text{erg s}^{-1}$. The background at this location is enhanced due to the scattering wings of N1 and SSS and due to the unresolved diffuse emission in the core of M31. By summing the counts in 3 pixel diameter circles placed in a ring equidistant from N1, we determined the background contribution from N1 and the diffuse emission to be 3.4 ± 2.3 counts at the location of M31*. In the same way we determined the contribution from SSS to be 2 ± 1.9 counts. The 13 counts at the position of M31* therefore represents a $\sim 2.5\sigma$ detection. While very suggestive, this clearly needs confirmation. Alternatively we may use the data to derive a 3σ upper limit to the luminosity that is only slightly higher at $L_{\text{X}} = 3.6 \times 10^{35} \text{erg s}^{-1}$.

2.2.1. Registering the ACS and HRC Images

The ACS image described above contains both mita213 and M31*, but no other globular clusters. We therefore used mita213 to register the two images, and using the same type of error analysis as for the ACIS-I/WFPC images we find a 1σ position error of 0.11''. We note that because we are limited to a single registration object in this case we are not able to check for roll or plate scale errors. However, the fact that these were measured to be negligible for the ACIS-I/WFPC case indicates that they should be negligible here as well.

3. Discussion

Having resolved M31* from the surrounding point and diffuse X-ray sources we can now investigate the accretion properties of this nearby SMBH. The presence of hot and truly diffuse emission component in the core of M31 was first noted in *Einstein* observations (Trinchieri & Fabbiano 1991) and later confirmed with *ROSAT* (Primini et al. 1993), *XMM-Newton* (Shirey et al. 2001), and *Chandra* (Dosaj et al. 2002) observations. Any of this gas within the Bondi radius of the SMBH will accrete and possibly generate accretion luminosity. In order to compute the Bondi accretion rate we use the X-ray observations to estimate the temperature and density of this gas.

The temperature in the inner $\sim 5'$ has been estimated as ~ 0.35 keV based on *XMM-Newton* observations (Shirey et al. 2001) and been found to fall radially from 0.50 keV to 0.26 keV based on *Chandra* ACIS-I observations (Dosaj et al. 2002). Recently Takahashi et al. (2004) has combined *XMM-Newton* and *Chandra* ACIS-S observations to reveal that there are three distinct soft temperature components which have slightly different radial surface brightness variations, therefore explaining the slight discrepancy between the earlier two results. The dominant component in terms of emission measure and particle density has a temperature of ~ 0.3 keV.

The density of the diffuse gas near the SMBH can be estimated from the emission measure and surface brightness profile fits. Dosaj et al. (2002) measured the profile within the central $1'$ and find that it appears to flatten. They estimate a gas density of $\rho \sim 0.1 \text{ cm}^{-3}$. Takahashi et al. (2004) measure a separate surface brightness profile for each of the three temperature components they find, in $1'$ bins. Summing the flux from all three in the inner bin also indicates a density of $\sim 0.1 \text{ cm}^{-3}$ within $1'$ (~ 200 pc) of M31*. We note that this density is similar to that found in other nearby galaxies (Di Matteo et al. 2003; Loewenstein et al. 2001), but a factor of ten below that found near Sgr A* (Baganoff et al. 2003).

In computing the Bondi radius we follow the prescription of Baganoff et al. (2003) exactly, thereby allowing direct comparisons. The radius is $R_B = 2GM_{BH}/c_s^2$, where the sound speed $c_s = (\gamma kT/\mu m_H)^{1/2}$. Here the adiabatic index $\gamma = 5/3$ and the mean atomic weight of the gas $\mu = 0.7$. Given the density and pressure in the previous paragraphs and using the dominant temperature component of 0.3 keV, we find for M31* $R_B = 3.4$ pc, or $R_B = 0.9''$ at the 780 kpc distance of M31.

This can be compared with Sgr A* with $R_B = 0.072$ pc or $= 1.8''$ (Baganoff et al. 2003) and M87 with $R_B = 1.7''$ (Di Matteo et al. 2003). Loewenstein et al. (2001) have computed the Bondi radii for a set of nearby elliptical galaxies in which the temperature of the central diffuse gas can be measured, and find $0.049'' < R_B < 0.36''$ for this set. Assuming similar

temperatures, we computed the apparent angular radii of the SMBH in the definitive study of such objects in nearby galaxies (Magorrian et al. 1998) and find in all cases $R_B \lesssim 0.4''$ ($R_B \sim 0.4''$ only for NGC 4486, NGC 4649, and NGC 4889; for the majority of the objects $R_B < 0.1''$).

While resolving the Bondi radius allows one to securely measure the magnitude of the accretion flow, the next most fundamental number is likely the ratio of the observed luminosity to the Bondi luminosity $L_B = 0.1\dot{M}_B c^2$. The Bondi luminosity is the maximum luminosity that one could expect, assuming that the initially spherical flow eventually forms a classical thin accretion disk. Following Baganoff, $\dot{M}_B = \pi(GM_{BH})^2 \rho c_s^{-3} = 3.4 \times 10^{20} \text{g s}^{-1}$ where $\rho = n_e \mu m_H$. For M31* we compute $L_B = 3 \times 10^{40} \text{erg s}^{-1}$. The possible detection of M31* indicates $L_X = 3 \times 10^{35} \text{erg s}^{-1}$ and therefore $L_X/L_B = 1 \times 10^{-5}$.

The Bondi radii and L_X/L_B for nearby SMBH are plotted in Figure 5. This figure shows that M31* is one of only three nearby SMBH with a Bondi radius larger than the *Chandra* resolution. These objects therefore allow the most secure measurements of the accretion rate at the outer edge of the flow. Knowing this, we may be able to determine if the flows contain winds (ADIOS) convection (CDAFs), or if the emission is dominated by jet processes (Falcke 2001) rather than thermal emission. For example, Gallo et al. (2003) recently found that in quiescent stellar mass black holes there is a correlation between the radio and X-ray luminosity $L_R \propto L_X^{0.7}$. The correlation also applies in AGN (Merloni et al. 2003) but the normalization of the correlation depends on the mass of the SMBH powering the AGN. Yuan and Cui (2005) model these correlations in terms of emission from a jet, predicting that the correlation should steepen at the very low luminosity found here for M31*. The observed X-ray and radio luminosity of M31* fall on this steeper correlation of $L_R \propto L_X^{1.23}$ (Yuan & Cui 2005). Interpreted in terms of this model, our observations imply that both the X-ray and radio emission from M31* are dominated by emission from an un-resolved, low bulk Lorentz factor (< 1.2) outflow.

While objects on the extreme right of Figure 5 provide the most secure measurements of the accretion rate because R_B is resolved, those at the extreme lower end provide the most severe constraints on the accretion processes because the flows are the most under-luminous. We see that M31* is exceeded only by Sgr A* in providing simultaneously the most secure and most severe constraints. If our possible detection is incorrect, then the true luminosity of M31* must be even lower. As an example, we show in Figure 5 the upper limit possible from a 200 ks *Chandra* HRC-I observation, which is a factor of 10 below our possible detection. We plan such a deep observation during *Chandra* AO6. Such a low L_X/L_R ratio may be difficult to explain in terms of the jet model proposed by Yuan & Cui (2005).

4. Summary

The observations we present herein provide evidence for a marginal detection of X-ray emission from M31* at the level of $L_X = 3 \times 10^{35} \text{erg s}^{-1}$, which is 10^{-5} times below the expected Bondi accretion luminosity. The Bondi accretion radius of the diffuse X-ray plasma surrounding M31* is $R_B = 0.9''$, larger than the resolution of the X-ray observations. The estimated Bondi accretion rate is therefore very securely known. These two points taken together show that M31* is exceeded only by Sgr A* in providing the most secure and severe evidence for a radiatively inefficient accretion flows in SMBHs.

This work was supported in part by NASA LTSA grant NAG5-10889 and Contract NAS8-39073 to the Chandra X-ray Center.

REFERENCES

- Baganoff, F. K., Maeda, Y., Morris, M., Bautz, M. W., Brandt, W. N., Cui, W., Doty, J. P., Feigelson, E. D., Garmire, G. P., Pravdo, S. H., Ricker, G. R., & Townsley, L. K. 2003, *ApJ*, 591, 891
- Barmby, P. & Huchra, J. P. 2001, *AJ*, 122, 2458
- Crane, P. C., Dickel, J. R., & Cowan, J. J. 1992, *ApJ*, 390, L9
- Di Matteo, T., Allen, S. W., Fabian, A. C., Wilson, A. S., & Young, A. J. 2003, *ApJ*, 582, 133
- Dosaj, A., Garcia, M., Forman, W., Jones, C., Kong, A., di Stefano, R., Primini, F., & Murray, S. 2002, in *ASP Conf. Ser. 262: The High Energy Universe at Sharp Focus: Chandra Science*, 147–+
- Gallo, E., Fender, R. P., & Pooley, G. G. 2003, *MNRAS*, 344, 60
- Garcia, M. R., Kong, A., Primini, F. A., Barmby, P., Di Stefano, R., McClintock, J. E., & Murray, S. S. 2001, in *Two Years of Science with Chandra, Abstracts from the Symposium held in Washington, DC, 5-7 September, 2001*.
- Garcia, M. R., Murray, S. S., Primini, F. A., Forman, W. R., McClintock, J. E., & Jones, C. 2000, *ApJ*, 537, L23
- Kaaret, P. 2002, *ApJ*, 578, 114
- Kong, A. K. H., Garcia, M. R., Primini, F. A., Murray, S. S., Di Stefano, R., & McClintock, J. E. 2002, *ApJ*, 577, 738

- Kormendy, J. & Bender, R. 1999, *ApJ*, 522, 772
- Loewenstein, M., Mushotzky, R. F., Angelini, L., Arnaud, K. A., & Quataert, E. 2001, *ApJ*, 555, L21
- Macri, L. M., Calzetti, D., Freedman, W. L., Gibson, B. K., Graham, J. A., Huchra, J. P., Hughes, S. M. G., Madore, B. F., Mould, J. R., Persson, S. E., & Stetson, P. B. 2001, *ApJ*, 549, 721
- Magnier, E. A. 1993, Ph.D. Thesis
- Magorrian, J., Tremaine, S., Richstone, D., Bender, R., Bower, G., Dressler, A., Faber, S. M., Gebhardt, K., Green, R., Grillmair, C., Kormendy, J., & Lauer, T. 1998, *AJ*, 115, 2285
- Merloni, A., Heinz, S., & di Matteo, T. 2003, *MNRAS*, 345, 1057
- Murray, S. S., Garcia, M. R., & Primini, F. A. 1999, *IAU Circ.*, 7291, 1
- Perna, R., Narayan, R., Rybicki, G., Stella, L., & Treves, A. 2003, *ApJ*, 594, 936
- Primini, F. A., Forman, W., & Jones, C. 1993, *ApJ*, 410, 615
- Shirey, R., Soria, R., Borozdin, K., Osborne, J. P., Tiengo, A., Guainazzi, M., Hayter, C., La Palombara, N., Mason, K., Molendi, S., Paerels, F., Pietsch, W., Priedhorsky, W., Read, A. M., Watson, M. G., & West, R. G. 2001, *A&A*, 365, L195
- Stanek, K. Z. & Garnavich, P. M. 1998, *ApJ*, 503, L131+
- Takahashi, H., Okada, Y., Kokubun, M., & Makishima, K. 2004, *ApJ*, 615, 242
- Trinchieri, G. & Fabbiano, G. 1991, *ApJ*, 382, 82
- Yuan, F. & Cui, W. 2005, *ApJ*, astro
- Yuan, F., Quataert, E., & Narayan, R. 2003, *ApJ*, 598, 301

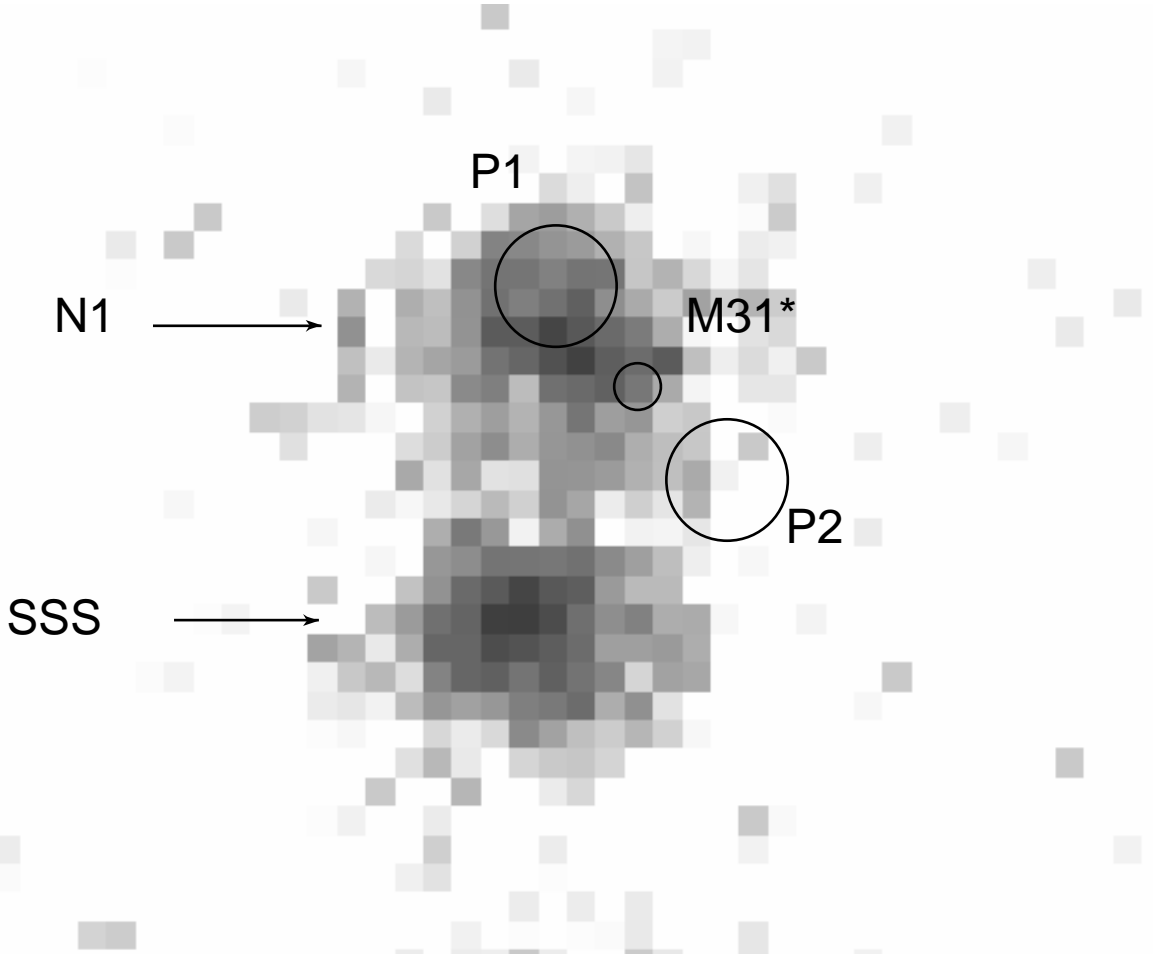


Fig. 1.— The 35.7 ks merged ACIS image of the M31 nucleus with $1/8''$ pixels. The sources labeled N1 and SSS are known as CXOM31 J004244.3+411608/r1-10 and CXOM31 J004244.3+411607/r1-9 in Kong et al. (2002). The distance between these two sources is $1.2''$. The supersoft source SSS is fainter in this epoch than in the HRC image. The position of M31* is marked with a small ($0.1''$ radius = 1σ position error) circle. The approximate locations of the diffuse double nucleus P1/P2 are marked with larger circles.

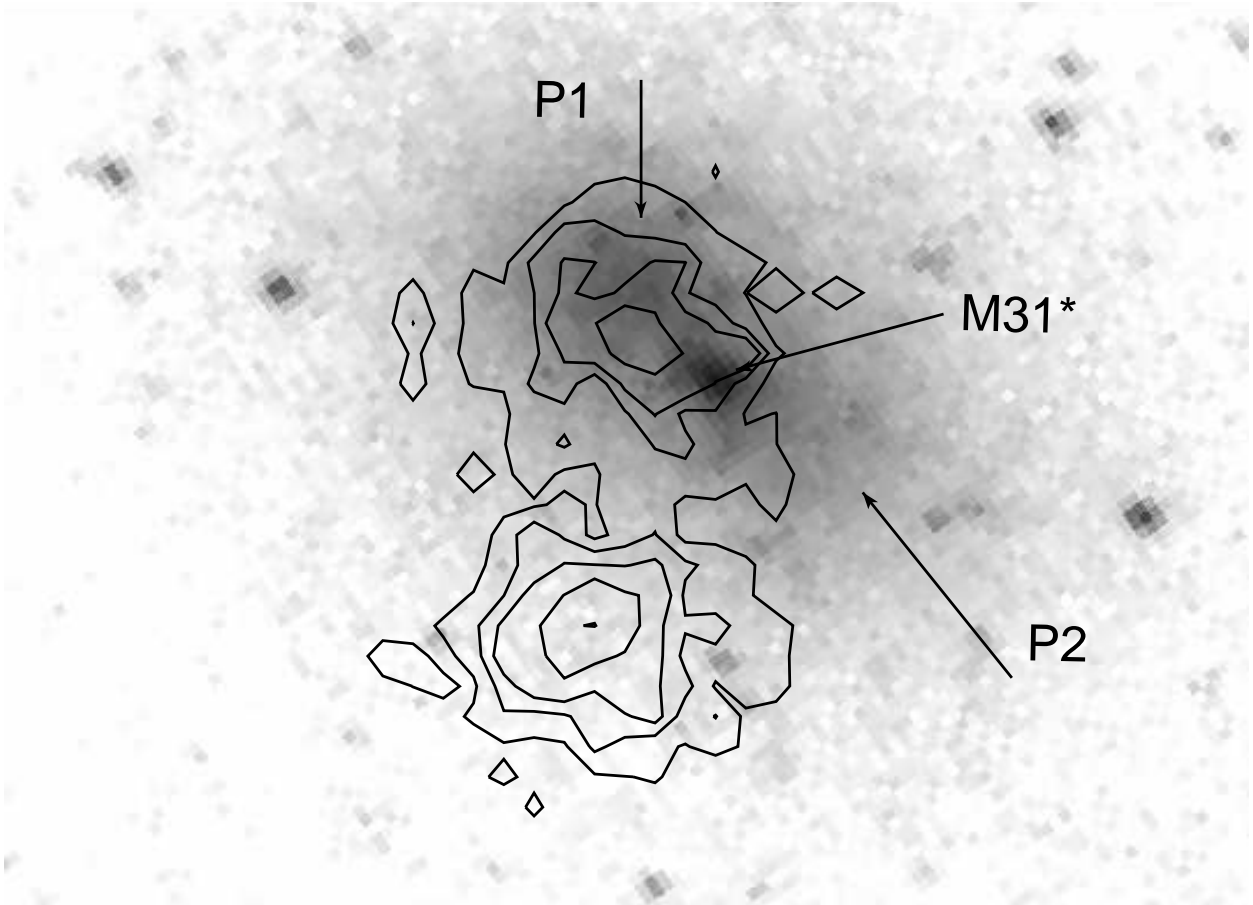


Fig. 2.— An archival F300W PC2 image of the M31 nucleus with ACIS contours overlaid. The double nucleus P1/P2 is marked, but P2 is only faintly discernible due to its red color. M31* is the brightest object near the center. The ACIS contours show that M31* is not coincident with any of the bright X-ray sources. While these contours do not show a resolved source at the position of M31*, the slightly elongated contours in its direction are consistent with the flux of M31* indicated by the HRC image.

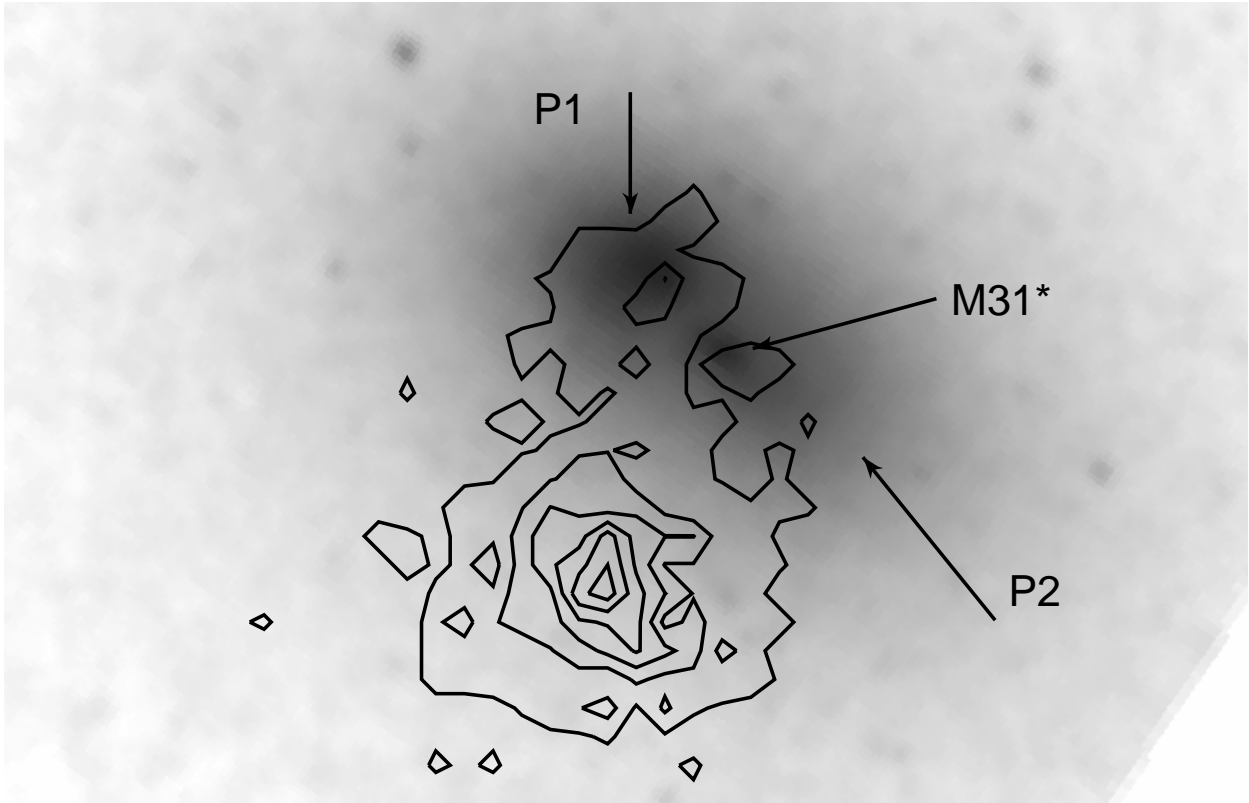


Fig. 3.— The HST/ACS image of the M31 nucleus with HRC contours overlaid. The double nucleus P1/P2 is marked, but P2 is only faintly discernible on this B-band image due to its red color. M31* is the more compact, bright object to the lower right of P1. There is a clear separate contour consistent with the position of M31*, indicating a possible X-ray detection of this SMBH. The plate scale here is the same as in Figure 2.

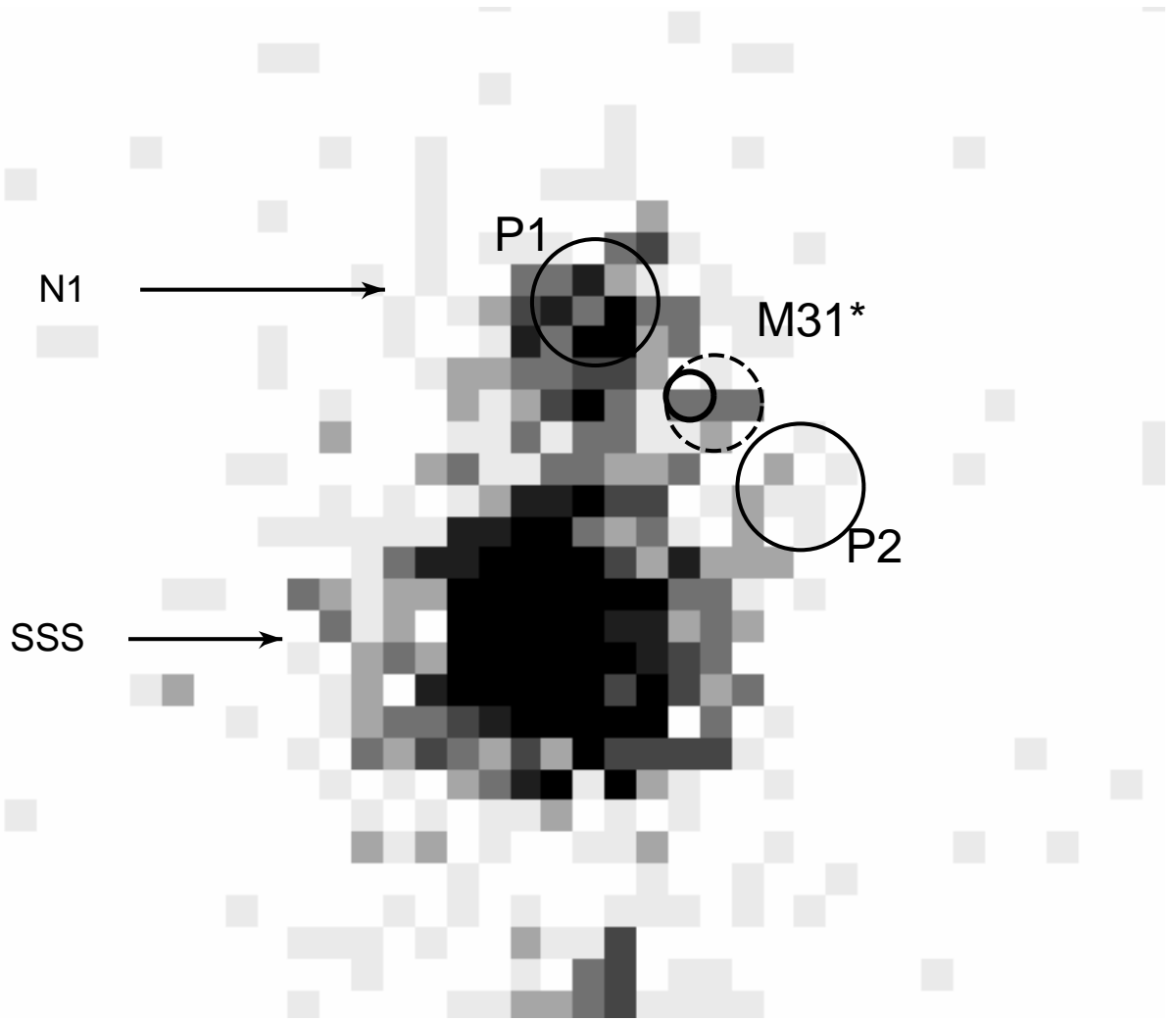


Fig. 4.— The 47 ks HRC image of the M31 nucleus, with $1/8''$ pixels. The source at the top is N1, the brighter source in the center is the super-soft source SSS. The position of M31* is marked with a small ($0.1''$ radius = 1σ position error) heavy circle in the center. The source outlined with the dashed circle is clearly consistent with the position of M31*. There are 13 counts within this dashed circle. The locations of the diffuse double nucleus P1/P2 are schematically indicated with the larger circles.

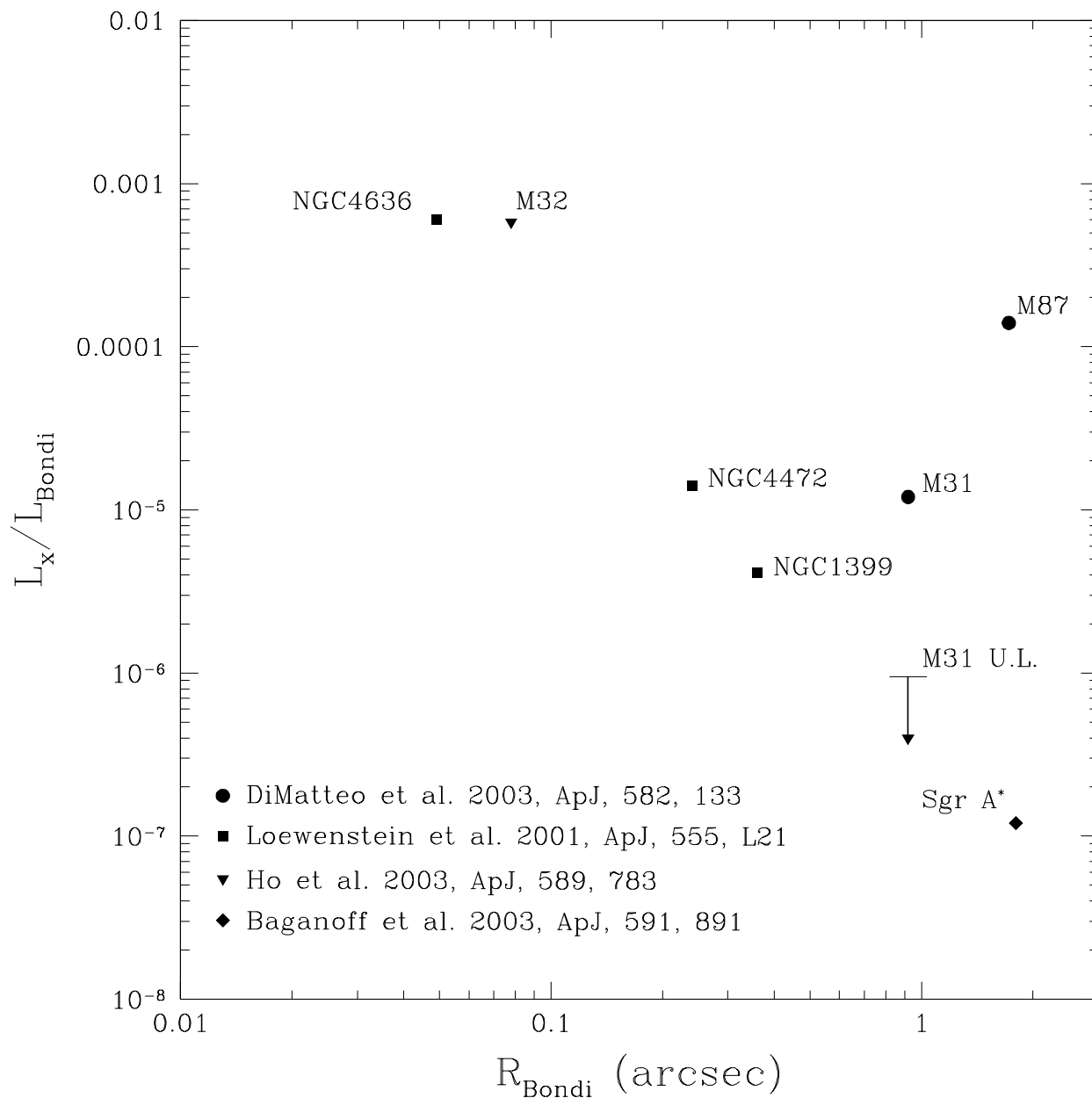


Fig. 5.— The Bondi radii of nearby SMBH vs. their apparent X-ray luminosity (or upper limits) in units of the expected Bondi luminosity. The only two extra-galactic SMBH with resolvable radii are M31* and M87. The point labeled M31 corresponds to the possible detection reported herein, and the line labeled 'M31 U.L.' corresponds to the upper limit possible with a 200 ks *Chandra* HRC-I observation.